Research Square

Preprints are preliminary reports that have not undergone peer review.
They should not be considered conclusive, used to inform clinical practice,
or referenced by the media as validated information.

# A fuzzy-to-ordered switch in the binding mode of the disordered regulator HigA2 mediates a ratio-sensing gene circuit

**San Hadži**

san.hadzi@fkkt.uni-lj.si

Department of Physical Chemistry, Faculty of Chemistry and Chemical Technology, University of Ljubljana https://orcid.org/0000-0002-5615-7918

**Zala Živič**

University of Ljubljana https://orcid.org/0000-0001-9044-3064

**Tadej Medved**

Department of Physical Chemistry, Faculty of Chemistry and Chemical Technology, University of Ljubljana https://orcid.org/0009-0006-4022-7068

**Zala Urbič**

University of Ljubljana, Faculty of Chemistry and Chemical Technology

**Luka Lipoglavšek**

Department of Microbiology, Biotechnical Faculty, University of Ljubljana

**Martin Gazvoda**

University of Ljubljana https://orcid.org/0000-0003-3421-0682

**Uroš Zavrtanik**

Department of Physical Chemistry, Faculty of Chemistry and Chemical Technology, University of Ljubljana, https://orcid.org/0000-0001-7445-6850

**Remy Loris**

Structural Biology Brussels, Department of Biotechnology, Vrije Universiteit Brussel

**Jurij Lah**

University of Ljubljana, Faculty of Chemistry and Chemical Technology https://orcid.org/0000-0003-1021-3803

**Article**

**Keywords:**

**Posted Date:** June 2nd, 2026

**DOI:** https://doi.org/10.21203/rs.3.rs-9629881/v1

**License:** This work is licensed under a Creative Commons Attribution 4.0 International License.
Read Full License

**Additional Declarations:** There is **NO** Competing Interest.

---

# Abstract

For globular transcription factors (TFs), the link between structure, sequence, and the output of the gene circuit is well established. In contrast, the mechanistic roles of intrinsically disordered regions (IDRs) in TFs and their connection to function remain less understood. Here, we investigate the *higBA2* toxin-antitoxin module from the human pathogen *Vibrio cholerae*, where the HigA2 repressor binds its operator through fuzzy interactions mediated by the IDR. Expression of the cognate HigB2 toxin disrupts these interactions, triggering transcriptional de-repression. In the presence of the toxin, the HigA2 IDR instead engages in an ultra-tight, folding-upon-binding interaction with HigB2, reducing the HigA2 DNA-binding affinity. Gene activity mapping and mathematical modeling reveal that this dual binding logic -where the same IDR encodes both fuzzy and ordered modes- enables the *higBA2* circuit to sense and respond to the cellular toxin:antitoxin ratio. This mechanism, which does not require communicating binding sites on the operator, represents an alternative evolutionary solution for implementing ratio-sensing regulation in toxin-antitoxin modules.


# Introduction

In contrast to the highly complex transcription regulation in Eukaryotes, with multiple roles for intrinsically disordered regions (IDRs),[1–4] bacterial transcription networks often display a more deterministic, digital-like logic in which input–output relationships are well defined, with the *lac* operon serving as paradigm.[5,6] Consistent with these differences, intrinsic disorder is much less prevalent in bacteria: only ~ 5% of bacterial transcription factors contain IDRs, compared with ~ 80% in eukaryotes.[7]

A notable exception are bacterial toxin–antitoxin (TA) systems, where the functional roles of IDRs are well-established.[8] TA systems are small genetic circuits widespread in bacteria and archaea.[9] In most cases they encode a protein toxin and its cognate antitoxin, though variants with RNA toxins/antitoxins also exist. The biological role(s) of TA systems remain heavily debated, with recent data pointing in their role as phage-defence systems.[10] Activated toxins result in cellular shutdown by targeting essential cellular processes, most often translation via mRNA or tRNA cleavage, modification of translation factors and DNA replication.[11] Antitoxins counteract toxins through direct binding, and in many families they are organized as bimodular proteins with an IDR fused to the globular DNA-binding domain.[8] These IDRs play a crucial role in toxin neutralization by forming ultra-tight complexes via folding-upon-binding mechanisms, often reaching picomolar affinities. For example, the HigB2-HigA2 interaction reaches picomolar affinity, despite the entropic cost associated with IDR folding.[12]

The functionality of antitoxin IDRs extends beyond toxin neutralization and is crucial for transcription regulation.[13] In several structurally unrelated TA families, transcriptional control is mediated by the regulation mechanism called conditional cooperativity, where toxin can act either as co-repressor or de-repressor depending on the molar toxin:antitoxin ratio. At low toxin:antitoxin ratios repressing toxin–antitoxin oligomers are formed through bridging toxins with IDR, and these bind to the multi-site

operators with high-affinity. Above a certain toxin threshold, these repressor complexes dissociate, leading to transcription activation. Such ratio-sensing regulatory mechanism is believed to maintain a constant excess of antitoxin over toxin as well as preventing stochastic spikes in toxin concentration.[14,15]

The *higBA* family of toxin-antitoxin modules induce cell growth arrest via cleavage of mRNA in the ribosomal A-site similar to RelE.[16–18] Previously, we found that the transcription of the chromosomally encoded *higBA2* module from *Vibrio cholerae* is regulated via operator region containing only a single palindromic binding site (Fig. 1A), making it incompatible with the classical conditional cooperativity mechanism that requires multiple sites on the operator.[19] Notably, the regulator HigA2 antitoxin contains an N-terminal IDR that is essential for both toxin neutralization[20] and transcription repression.[19] As a transcription factor HigA2 binds to DNA via its globular domain which provides a base-specific readout, while its IDR remains disordered and enhances binding affinity through dynamic, transient IDR-DNA interactions forming a prototypical fuzzy complex.[19] However, the role of the HigB2 toxin in the *higBA2* autoregulation has remained unresolved.

Here, we show that HigB2 toxin functions as a transcriptional de-repressor through a mechanism where both HigB2 and the operator DNA compete for binding to HigA2 IDR. In the absence of toxin, the IDR forms fuzzy interactions with DNA enhancing the transcription repression. Upon increase in toxin level, IDR becomes sequestered into an ordered, high-affinity toxin–antitoxin complex, reducing the DNA binding affinity. The transcriptional on/off switch results from competitive binding of the IDR to DNA versus toxin. Using quantitative model and *in vivo* experiments we show that *higBA2* expression is regulated by a ratio-sensitive regulatory mechanism, despite being limited with a single-site operator architecture. These findings reveal that distinct toxin-antitoxin mechanisms converge on similar regulatory phenotype and demonstrate the emergence of a new gene circuit functionality based on the dual binding logic of a disordered transcription factor.

## RESULTS

# HigB2 toxin alleviates HigA2-mediated repression of transcription

HigA2 antitoxin acts as the transcriptional repressor by binding to the single palindromic site on the *higBA2* operon (Fig. 1A). Its globular C-terminal DNA-binding domain is employed for the DNA sequence readout, while its disordered N-terminal region strengthens the binding through fuzzy interactions to the DNA.[19] To understand the role that the toxin HigB2 plays in transcription regulation, we designed a reporter vector expressing fluorescent *mRFP1* under the *higBA2* promotor $P_{higBA2}$ (Fig. 1B). In absence of any HigA2 or HigB2, cells containing $P_{higBA2}$-*mRFP1* exhibit a strong fluorescence, indicating *mRFP1* expression. The construct encoding an additional HigA2 antitoxin under a constitutive promotor gives lower signal, indicating HigA2-mediated repression (Fig. 1B). Conversely, in the construct expressing

both HigA2 and HigB2 we observe high fluorescence values (Fig. 1B), indicating that the HigB2 toxin acts as de-repressor. As a control, we further measured cells constitutively expressing inactive HigB2 only, which gives similar values as $P_{higBA2}$-*mRFP1* (Fig. 1B). Flow cytometry data of these constructs confirm that HigB2 acts as de-repressor of *higBA2* operon also at the single-cell level (Fig. 1C), in correspondence with the batch measurements.

To validate the HigB2 de-repressor activity in real time, we designed a vector system where the expression of HigB2 or HigA2 can be induced independently using small-molecule inducers (Fig. 1D). We implemented additional modifications to the vector to provide unimodal (rather than all-or-none) protein expression upon IPTG or arabinose induction.[21] Cells without inductors express sfGFP from the *higBA2* promotor (gray curve, Fig. 1D), while cells grown in the presence of IPTG show reduced sfGFP expression due to HigA2 repression (blue curve, Fig. 1D). Upon addition of arabinose into cells grown in presence of IPTG, we observe a clear increase in fluorescence values (pink curve, Fig. 1D). This shows that HigB2 alleviates HigA2 repression in time-dependent manner and reinitiates sfGFP expression.

To investigate the interplay between HigB2, HigA2 and the operator DNA *in vitro* we purified both proteins and investigated binding using electrophoretic mobility shift assay (EMSA). Addition of HigA2 or HigB2-HigA2 to the 45 bp operator fragment leads to appearance of shifted bands corresponding to protein-DNA complex, with higher concentrations of HigB2-HigA2 required for full operator saturation (Fig. 1E). This suggests that the HigB2-HigA2 complex can still bind the operator, but with lower affinity than HigA2 on its own. To compare the binding affinities quantitatively we performed fluorescence anisotropy titrations using labelled DNA duplex (Fig. 1F). The binding isotherm for HigA2 suggests high affinity binding to DNA operator ($K_D$=10 ± 1 nM), while the binding affinity of HigB2-HigA2 complex is over an order of magnitude lower ($K_D$=212 ± 4 nM). Although purified HigB2-HigA2 complex shows residual binding to the operator, *in vivo* experiments suggest that this affinity is too weak for efficient repression within the cellular concentration range. Collectively, these data support that HigB2 toxin acts as de-repressor *in vivo* and *in vitro* by reducing the DNA-binding affinity of HigA2 antitoxin.

## Structure of the low affinity HigB2-HigA2-operator complex

To delineate the mechanism by which toxin decreases the affinity for operator, we determined the crystal structure of the HigB2-HigA2-operator complex at 3.3 Å resolution (Fig. 2A, **Table S1**). In this complex the DNA molecule is bent to a similar angle as in the HigA2-DNA complex.[19] The majority of the protein-DNA contacts are restricted to the HigA2 globular domain and remain essentially identical to those observed in the HigA2-DNA complex reported previously (Fig. 2A**_inset2, Figure S1**). Given the close proximity between toxin HigB2 and DNA, there are surprisingly few contacts between both molecules. These are limited to the HigB2 short loop connecting helix α2 and strand β2, where Lys36 and Arg48 interact with the phosphate backbone which is likely compensated by the repulsive interaction of the adjacent Asp39 and phosphate group (Fig. 2A**_inset1**). The HigB2-HigA2-operator structure however reveals a major change in the global conformation of the HigB2-HigA2 tetramer upon binding to the

operator (Fig. 2B). In comparison to the unbound HigB2-HigA2 extended tetramer,[22] the DNA-bound tetramer adopts a bent, V-shaped conformation. The angle between the two symmetric halves of tetramer decreases from 150° to 110° in DNA-bound state compared to the free state (Fig. 2B). This change essentially consists of a rigid body movement of HigB2 relative to HigA2 through sliding of HigB2 α2 helix along the groove formed by HigA2 α2 and α3 helices. The structural superposition of the extended (free) HigB2-HigA2 form to DNA operator shows that tetramer bending is required to prevent direct steric clashes between the HigB2 toxin and DNA molecule (Fig. 2C).

## The HigB2-HigA2 tetramer is flexible is solution

The observed conformational change of HigB2-HigA2 alludes to the possible mechanism by which the decrease in DNA-binding affinity in presence of HigB2 coming from the energetically unfavourable tetramer bending. Several lines of evidence however indicate that the tetramer is a flexible molecule, which would be inconsistent with a high energy penalty for tetramer bending. The first indication of flexibility comes from the AlphaFold3 prediction of the HigB2-HigA2 tetramer structure. While the predicted structures of individual HigB2 and HigA2 agree with the experimental ones, their relative position in the tetramer sample the bending angles between 110° and 150°, which is within the range of two conformations observed crystallographically (Fig. 3A). Motivated by this finding we used normal mode analysis to examine low-frequency dynamics of the HigB2-HigA2 tetramer. Harmonic elastic network model[23] indicates that the largest normal mode is associated with the hinge-bending motion of the HigB2 relative to HigA2 (Fig. 3B, **Table S2, Movie S1**). This is consistent with the dynamic sampling of conformations between the extended and bent form, as captured in the AlphaFold3 models. To corroborate these predictions, we measured small-angle-X-ray scattering (SAXS) of the HigB2-HigA2 tetramer devoid of purification tags. The experimental SAXS curve is best described by the weighted average of theoretical scattering profiles belonging to the extended/free and the bent/DNA-bound conformations (Fig. 3C). Taken together, these observations are consistent with the flexible structure that dynamically samples bent and extended conformations at minimal energetic cost.

## Transcriptional de-repression is not caused by the HigB2-HigA2 conformational switch

To directly examine whether HigB2–HigA2 tetramer bending decreases operator affinity, we designed tetramer variants that are conformational restrained into the bent, 110 ° conformation. For binding of these variants to DNA, any contribution due to tetramer bending would be thus excluded. Twelve residues from the HigB2-HigA2 interface were redesigned using ProteinMPNN and threaded onto the template structures followed by the relaxation and scoring with a custom Rosetta-based energy function (see Methods). These variants were then ranked to maximize the energy difference between 110° and 150° angle conformations and further filtered by the AlphaFold3-predicted scores (**Figure S2**). The top three sequences (variants HigB2-HigA2 110A to 110C, **Table S3**) were then further characterized. The

crystal structure of the 110A tetramer variant at 2 Å resolution exhibits the 110° angle between two tetramer halves, confirming the successful design of this bend tetramer (Fig. 3D). While the tetramer adopts the designed binding angle, we observed an additional lateral rotation in one tetramer half, which we attribute to the difference in crystal packing (**Figure S3**). Fluorescence anisotropy measurements show the binding affinity of the crystalized 110A variant for a 45 bp *higBA2* operator sequence to be the same as that of the native HigB2-HigA2 complex (Fig. 3E). This indicates that the conformational change induced by DNA binding has no influence on the operator affinity, consistent with the high flexibility of the complex. Similar affinities were also observed for the two other tetramer variants designed to exhibit a stabilized bent conformation (Fig. 3E, **Figure S4**).

## Disrupting fuzzy interactions reduces binding affinity of HigA2 to DNA

We next looked for an alternative explanation of HigB2-mediated loss in operator affinity, focusing on the N-terminal disordered antitoxin domain. The decrease in the DNA binding affinity could be explained by sequestering of the IDR from DNA. Loss of fuzzy IDR-DNA interactions would lead to the reduction of HigA2-DNA binding affinity. To test this hypothesis, we designed a $HigA2_{[3+][3-]}$ variant which binds to the operator independently of its IDR. Here, binding to DNA is mediated by the globular domain only, leaving the IDR to freely interact with toxin, which effectively decouples toxin binding from the DNA binding (Fig. 4A). Using *in vivo* repression as a readout we first screened for IDR mutations that disrupt fuzzy interactions with DNA, but not toxin binding. Several individual substitutions into negatively charged residues were observed to decrease repression ability, likely due to electrostatic repulsion to DNA (**Figure S5**). Combining three of these mutations (K24E, T26E, T29E) into the $HigA2_{[3-]}$ variant results in a complete loss of repression, indicating effective elimination of IDR-DNA fuzzy interactions (Fig. 4A). In a second step, we screened for mutations that would strengthen the interactions between the globular domain and DNA and could be used to restore the $HigA2_{[3-]}$ repression ability. Selected positions on the globular domain of native HigA2 were redesigned using ProteinMPNN, evaluated by the Rossetta scoring function and individually tested for repression (**Figure S5).** Several individual mutations improved repression and combination of E37R, V46R and S78N mutations in the $HigA2_{[3+]}$ variant shows stronger repression compared to the native HigA2. Introduction of these compensatory mutations into the $HigA2_{[3-]}$ background completely restores its repression (Fig. 4A). This $HigA2_{[3+][3-]}$ variant thus efficiently binds DNA without relying on fuzzy IDR-DNA interactions. We then used ITC to confirm that the binding affinity of $HigA2_{[3+][3-]}$ is nearly identical affinity that of native HigA2 while strong binding to HigB2 is also retained (**Figure S6**).

Given that the IDR of $HigA2_{[3+][3-]}$ is not involved in interactions with DNA, we expected that the resulting protein-DNA complex will have more expanded ensemble compared to that of native HigA2. To verify this hypothesis, we measured SAXS profiles of native and $HigA2_{[3+][3-]}$ variant in complex with the 33 bp long operator fragment. The $HigA2_{[3+][3-]}$ complex has larger radius of gyration (30.0 ± 0.1 Å) compared

native HigA2 (27.4 ± 0.1 Å) (**Table S4**). Distance distribution functions show that a more expanded ensemble for the $HigA2_{[3+][3-]}$ variant (Fig. 4B), confirming that IDR is less restricted and not involved in interactions with the DNA.

To test whether competitive binding of IDR to toxin or DNA is responsible for toxin-mediated de-repression we used EMSA. In this experiment the operator is first titrated with antitoxin (HigA2 or $HigA2_{[3+][3-]}$) to obtain the repressor complex, followed by toxin titration to test for the release of the repressor. For the native HigA2 increasing the amount of toxin results in the release of the HigA2-repressor complex (Fig. 4C), due to sequestering of the IDR from the DNA. In contrast, while $HigA2_{[3+][3-]}$ binds to the operator DNA, addition of toxin does not lead to the operator release, since the IDR is not involved in DNA binding and $HigA2_{[3+][3-]}$ lacks a mechanism by which its affinity is reduced (Fig. 4C). This confirms that in native *higBA2* the mechanism behind the toxin-mediated de-repression is due to the competition of IDR to bind either DNA or toxin (Fig. 4D).

# Transcription autoregulation acts a HigB2/HigA2 ratio-sensing gene circuit

The EMSA binding profile of native *higBA2* (Fig. 4C**)** resembles the ratio-dependent response observed for the toxin-antitoxin modules regulated by the conditional cooperativity mechanism, where the operon is repressed at sub-stoichiometric toxin:antitoxin ratios and free when the toxin level exceeds the antitoxin level.[24,25] These systems rely on two or more communicating antitoxin binding sites on the operator, while the *higBA2* operator contains only one binding site. To understand whether *higBA2* operates as a *bona fide* ratio-sensing circuit, we turned to mathematical modelling. We developed an equilibrium thermodynamic model of the *higBA2* circuit parametrized with the *in vitro* experimental affinities, which gives the steady-state concentration molecular species at given total concentration of toxin and antitoxin proteins. We then investigated how fractional occupancy of the *higBA2* operator, a proxy for transcription activity,[26,27] changes with the concentration HigB2 and HigA2 (Fig. 5A). The operator is largely saturated in the presence of about 50 HigA2 molecules (blue line, Fig. 5A, **left**), but a gradual increase in the HigB2 leads to operator release (black line, Fig. 5A, **left**). The concentration of HigB2 required for the operator release depends on the initial HigA2 concentration (indicated by the increasing offset in Fig. 5A, **left**). However, plotting these traces against the HigB2/HigA2 molar ratio as the common independent variable, shows that switching between free and repressed states depends primary on the molar ratio, with the 2:1 switching threshold independent of the absolute protein concentrations (Fig. 5A, **right**). This indicates that the *higBA2* circuit output depends on the HigB2:HigA2 molar ratio as input variable, not the absolute concertation. Using the equilibrium model we predicted the complete output *higBA2* circuit, which is represented as a two-dimensional heat map showing how operator occupancy (output) depends on the HigB2 and HigA2 level (Fig. 5B). Two distinct areas correspond to the active (free) and inactive (bound) operator state. These are separated by the diagonal switching front running along the 2:1 toxin:antitoxin molar ratio in a wide concertation range. Such diagonally separated output functions were observed for circuits with ratio-dependent regulation, for

example in regulation of sugar metabolism genes,[28] and in *ccdBA* toxin-antitoxin module regulated by conditional cooperativity mechanism.[20]

To validate our mathematical model *in vivo*, we used a low-copy number reporter system that enables precise titration of (inactive) HigB2 or HigA2 proteins using the arabinose and IPTG inducers, respectively.[21] To reproduce different ratios of toxin and antitoxin in cell, we grew *E. Coli* cells in plates supplemented with different concentration of arabinose and IPTG and measured sfGFP fluorescence as a readout of *higBA2* promoter activity. Addition of arabinose leads to higher fluorescence values, in line with the HigB2 de-repression, but the required arabinose concentration also depends on the IPTG levels (Fig. 5C). Significantly, the OD-normalized fluorescence values across the whole inducer concentration range shows a clear diagonal pattern closely matching the expected gene output predicted by mathematical model (Fig. 5D). Through immunodetection of protein tags by Western bolting we confirmed that both HigB2 and HigA2 are expressed in cells in presence of inducers (**Figure S7**) and also verified that the protein expression is uniform in the bacterial population using flow-cytometry (**Figure S8**). Collectively, mathematical modelling and *in vivo* mapping the gene output confirm that *higBA2* autoregulation operates as a ratio-sensing circuit, as the *higBA2* expression depends on the molar ratio of HigB2 and HigA2 proteins.

**Ratio-sensing higBA2-like circuit provides homeostatic control and speeds-up the recovery from the toxin-rich state**

The ratio-dependent regulation phenotype in *higBA2* is achieved through a unique circuit topology. To investigate the functional performance of such anti-cooperative circuit based on toxin de-repression only (Fig. 6A), we performed stochastic kinetic simulations with Gillespie algorithm. Based on previously used simulation setup,[14] we analysed how system's return to normal steady-state from the toxin-rich state induced by starvation (Fig. 6B, **Figure S9**). We then compared return dynamics (Fig. 6B, **inset**) for different circuit architectures: system without transcription regulation (NO), system with negative-feedback (NE), *higBA2*-like anti-cooperative regulation (AC), and conditional cooperativity regulation (CC) (Fig. 6A, **Figure S9**). While the return dynamics within each circuit is subjected to stochasticity, the distributions for different circuits exhibit clear differences in return dynamics (Fig. 6C). Circuits implementing ratio-dependent regulation phenotype (CC and AC) enable significantly faster recovery form the toxin-rich state, compared to circuits without regulation or with negative-feedback only (Fig. 6C). Interestingly, despite differences in circuit architecture the functional performance of AC and CC is essentially identical, indicating functional convergence of both circuits.

We next investigated how different circuit topologies respond to perturbations in toxin–antitoxin ratio by tracking the trajectories through which the system returns to its steady-state ratio. The system’s response to perturbations at different points is represented by a vector filed, where arrows correspond to the direction and speed of the response trajectory (Fig. 6D). Comparison of the AC and NE vector fields shows different responses, particularly when perturbations exceed the 2:1 toxin:antitoxin ratio, that is when free toxin is present (arrows above the diagonal line Fig. 6D). For the AC circuit that incorporates

ratio-sensitivity, the response prioritizes a decrease of the toxin:antitoxin ratio below the 2:1 threshold (indicated by vectors pointing to the 2:1 diagonal, Fig. 6D). The CC circuit has a similar response as AC (**Figure S10**). In contrast, for the simple negative feedback (NE) the response trajectories do not prioritize decrease in toxin:antitoxin ratio below 2:1 and take different path (Fig. 6D). The distribution of vector directions for different circuits (Fig. 6E) shows that for ratio-sensing phenotype (AC and CC circuits), trajectories are preferentially oriented perpendicular to the 2:1 diagonal (angle 90 °), indicating a homeostatic mechanism that dampens any spikes in free toxin concentration. Collectively, these data support that ratio-sensing autoregulation circuits based only on toxin de-repression (as in *higBA2*) are functional, give comparable performance as the canonical CC mechanism, and enable both fast recovery from toxin-dominated state and homeostatic control of the steady-state toxin:antitoxin ratio (Fig. 6F).

# DISCUSSION

Cells have gone to great lengths to regulate the activity of toxin-antitoxin systems, and IDRs play central roles in their functioning and regulation. IDR functions range from direct folding-upon-binding interactions that achieve picomolar binding affinities[12] to allosteric control,[25] bispecific IDR interactions on different toxins sites,[25,29] and IDR-mediated entropic exclusion principles.[30,31] Integration of direct toxin binding with transcription regulation is classically accomplished through conditional cooperativity, first described for *ccdBA*.[20,24] In these systems, toxin acts as co-repressor (positive cooperativity) or de-repressor (negative cooperativity), depending on the molar ratio, a principle later observed across several structurally unrelated families, such as *kid–kis, relBE, vapBC, phd–doc, ataRT*, and *relBE* .[32–35] At the molecular level, this relies on multiple communicating DNA binding sites, where toxin-antitoxin oligomers of different stoichiometries mediate repression through increased avidity, cooperativity, or improved binding site selectivity.[13] Formation of these oligomers is mediated by toxin-IDR interactions, while toxin excess disrupts these oligomers.[20,25,33] Kinetic simulations suggested that conditional cooperativity prevents accidental toxin spikes enables fast recovery from the persister state.[14,15]

The chromosomal *Vibrio Cholerae higBA2* module deviates from this paradigm: its operator contains a single binding site, seemingly incompatible with conditional cooperativity. Yet, as we show here, a functionally equivalent regulatory phenotype emerges through a distinct negative cooperativity mechanism, in which the HigA2 IDR binds to either to the toxin or to the DNA target through two mutually exclusive binding modes. Following the logic of conditional cooperativity, we suggest that transcriptional regulatory mechanisms with a ratio-dependent phenotype incorporating negative cooperativity - where the toxin decreases the antitoxin DNA-binding affinity- may be described as *anti-cooperative* mechanisms. Mathematical modelling, *in vivo* experiments, and stochastic kinetic simulations demonstrate that the *higBA2* anti-cooperative mechanism is a *bona fide* ratio-dependent circuit that reproduces the functional advantages of conditional cooperativity,[14] including fast recovery from toxin-rich state and homeostatic control of the toxin:antitoxin ratio. These observations further imply that other TA systems where toxins act strictly as de-repressors may also exhibit ratio-dependent behaviour. For example, in *mqsRA* from *E. coli*[36] and *graTA* form *P. putida*[30] the toxin sterically interferes with DNA-

binding, leading to complete de-repression, while in the *hicAB* module from *B. pseudomallei* the toxin rearranges the antitoxin DNA-binding domains, leading to reduced operator binding affinity.[34] Similarly, weak de-repression effects described for the plasmid-borne *Proteus vulgaris higBA* system[37] are likewise consistent with this broader anti-cooperative category, although quantitative models are still lacking.

The 40-amino-acids-long HigA2 IDR emerges as the key element enabling this regulatory innovation. In solution, this IDR is disordered with only a transient helix between residues 7 and 21[19,22], which predisposes the HigB2-bound structure, where this region forms an ordered α-helix. Such transient helical structures are commonly stabilized by the LxxxL motifs,[38] that is also present in HigA2. Folding-upon-binding to HigB2 creates a highly optimized picomolar-affinity protein–protein interface that compensates for the entropic penalty of IDR ordering, which on average reduces binding free energies by + 2 kcal/mol.[39,40] In contrast, DNA binding leaves the IDR fully disordered, yet its fuzzy interactions enhance DNA affinity by more than two orders of magnitude.[19] Transcription regulation employs dynamic, fuzzy interactions mediated by disordered regions,[41] that typically resist sequence-scrambling.[42] In contrast, HigA2 IDR sequence scrambling abolishes operator binding, indicating the presence of hidden specificity determinants within the otherwise degenerate fuzzy binding. Alanine scanning mutagenesis revealed two specificity clusters on HigA2 IDR, which rely on a combination of polar and hydrophobic residues to interact with DNA.[19]

Strikingly, the ordered and fuzzy binding modes partially overlap within the same IDR: binding to HigB2 toxin involves residues 2 to 31, while the fuzzy interaction with DNA includes the N-terminal cluster (residues 2–6) and a cluster bordering the globular domain (residues 24–32). A recent statistical-thermodynamic model rationalizes this duality through the spatial patterning of IDP hotspots and the energetic balance between interaction strength and folding propensity.[43] In the ordered HigB2-bound ensemble, interacting IDR hotspot residues are clustered and involved in strong interactions, while in fuzzy DNA-bound ensemble, hotspots are more dispersed and individual contributions are weaker. Thus, encoding multiple binding modes within the same IDR can be realized through strategic hotspot patterning and tuning of interaction strength.

Binding versatility is a hallmark of IDPs. Classic examples such as p53 and CREB commonly involve variations of partially helical or extended conformations, rather than truly opposed ordered vs fuzzy binding.[44–47] Besides HigA2, one of the few known parallels with directly opposed binding modes is the acidic activation domain of yeast Gal4: it binds the repressor Gal80 via ordered helical folding, but binds the Mediator subunit Med15 through fuzzy interactions mediated by multiple hydrophobic specificity clusters.[48,49] Such clusters of specificity are common in acidic activation domains in yeast TFs where hydrophobic residues important for activation are distributed in the disordered sequence with a net negative charge.[49] However, Gal4 IDR sequence also encodes an ordered, high-affinity binding mode when interacting with Gal80 repressor, folding into a short helical element.[50,51] A further example is the NTAIL region of the measles virus nucleoprotein, which undergoes folding-upon-binding to the phosphoprotein X-domain.[52] At the same time, the same region of NTAIL interacts with Hsp70 possibly

via alternative, potentially fuzzy interactions that are not stabilized by helix formation.[53] The mechanistic analogy between yeast TF IDRs, the viral NTAIL, and bacterial HigA2, based on a dual fuzzy/ordered binding logic represents a shared regulatory strategy across domains of life, enabling IDRs to act as versatile molecular switches that integrate environmental signals directly into gene regulatory circuits.

## Declarations

# ADDITIONAL INFORMATION

Supplementary information accompanies this paper.

# AUTHOR CONTRIBUTIONS

Z.Ž. designed and prepared all constructs and proteins and performed biophysical and *in vivo* experiments. T.M. preformed protein design. Z.U. preformed kinetic simulations. S.H performed structural analysis. R.L., J.L., M.G. and S.H. acquired funding. S.H wrote the draft with assistance of Z.Ž, T.M and Z.U. All authors discussed the results, contributed to data analysis, revision and editing of the manuscript. S.H. designed the study and supervised the project.

# ACKNOWLEDGEMENTS

This work was supported by Slovenian Research Agency through grants P1-0201 and J1-50026. The authors would also like to acknowledge the use of beamtime at PROXIMA 1, PROXIMA 2 and SWING beamlines (synchrotron SOLEIL, St-Aubin, France) and their respective staff for help.

# DATA AVAILABILITY

All the crystallographic structural data has been deposited into the Protein Data Bank (www.rcsb.org) under the accession codes 9TV9 (designed HigB2-HigA2 tetramer variant) and 8A0X (HigB2-HigA2-Opr31). Experimental SAXS data is deposited in SASDB under accession codes SASDEV6, SASDER7 and SASDEW6.

## References

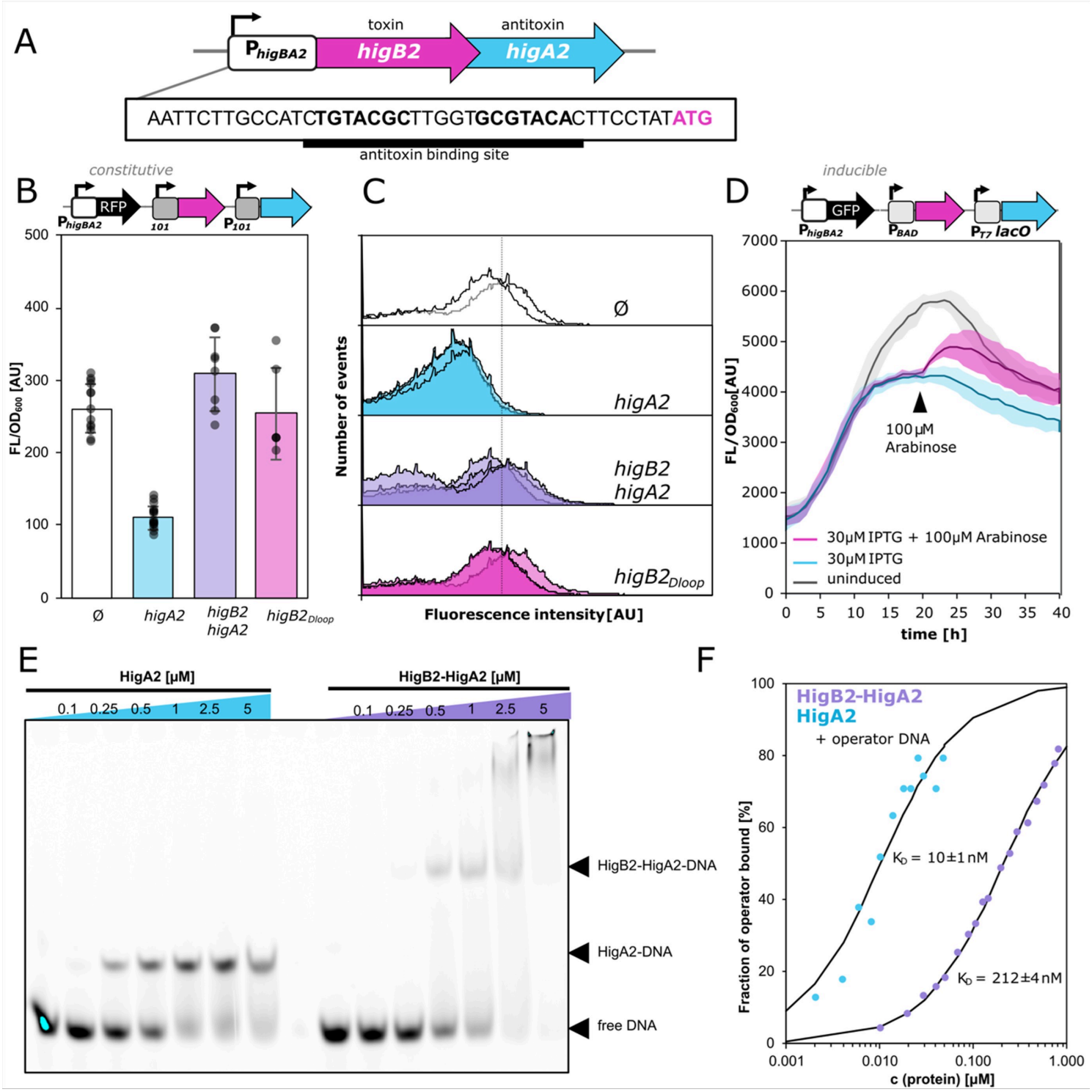
1. Pei G, Lyons H, Li P, Sabari BR (2025) Transcription regulation by biomolecular condensates. Nat Rev Mol Cell Biol 26:213–236
2. Ferrie JJ, Karr JP, Tjian R, Darzacq X (2022) Structure-function relationships in eukaryotic transcription factors: The role of intrinsically disordered regions in gene regulation. Mol Cell 82:3970–3984

3. Holehouse AS, Kragelund BB (2024) The molecular basis for cellular function of intrinsically disordered protein regions. Nat Rev Mol Cell Biol 25:187–211
4. Jonas F, Navon Y, Barkai N (2025) Intrinsically disordered regions as facilitators of the transcription factor target search. Nat Rev Genet 26:424–435
5. Bervoets I, Charlier D (2019) Diversity, versatility and complexity of bacterial gene regulation mechanisms: opportunities and drawbacks for applications in synthetic biology. FEMS Microbiol Rev 43:304–339
6. Yildirim N, Mackey MC (2003) Feedback Regulation in the Lactose Operon: A Mathematical Modeling Study and Comparison with Experimental Data. Biophys J 84:2841–2851
7. Liu J et al (2006) Intrinsic Disorder in Transcription Factors. Biochemistry 45:6873–6888
8. Loris R, Garcia-Pino A (2014) Disorder- and Dynamics-Based Regulatory Mechanisms in Toxin–Antitoxin Modules. Chem Rev 114:6933–6947
9. Jurėnas D, Fraikin N, Goormaghtigh F, Van Melderen L (2022) Biology and evolution of bacterial toxin–antitoxin systems. Nat Rev Microbiol 20:335–350
10. LeRoux M, Laub MT (2022) Toxin-Antitoxin Systems as Phage Defense Elements. Annu Rev Microbiol 76:21–43
11. Harms A, Brodersen DE, Mitarai N, Gerdes K (2018) Toxins, Targets, and Triggers: An Overview of Toxin-Antitoxin Biology. Mol Cell 70:768–784
12. Zavrtanik U, Hadži S, Lah J (2021) Unraveling the Thermodynamics of Ultra-tight Binding of Intrinsically Disordered Proteins. Front Mol Biosci 8
13. De Bruyn P, Girardin Y, Loris R (2021) Prokaryote toxin–antitoxin modules: Complex regulation of an unclear function. Protein Sci 30:1103–1113
14. Cataudella I, Trusina A, Sneppen K, Gerdes K, Mitarai N (2012) Conditional cooperativity in toxin–antitoxin regulation prevents random toxin activation and promotes fast translational recovery. Nucleic Acids Res 40:6424–6434
15. Gelens L, Hill L, Vandervelde A, Danckaert J, Loris R (2013) A General Model for Toxin-Antitoxin Module Dynamics Can Explain Persister Cell Formation in E. coli. PLoS Comput Biol 9:e1003190
16. Schureck MA, Dunkle JA, Maehigashi T, Miles SJ, Dunham CM (2015) Defining the mRNA recognition signature of a bacterial toxin protein. *Proceedings of the National Academy of Sciences* 112, 13862–13867
17. Neubauer C et al (2009) The Structural Basis for mRNA Recognition and Cleavage by the Ribosome-Dependent Endonuclease RelE. Cell 139:1084–1095
18. Mansour M et al (2022) Substrate recognition and cryo-EM structure of the ribosome-bound TAC toxin of Mycobacterium tuberculosis. Nat Commun 13:2641
19. Hadži S et al (2024) Fuzzy recognition by the prokaryotic transcription factor HigA2 from Vibrio cholerae. Nat Commun 15:3105

20. Vandervelde A et al (2017) Molecular mechanism governing ratio-dependent transcription regulation in the ccdAB operon. Nucleic Acids Res 45:2937–2950
21. Živič Z, Lipoglavšek L, Lah J, Hadži S (2025) A single vector system for tunable and homogeneous dual gene expression in Escherichia coli. Sci Rep 15:99
22. Hadži S et al (2017) Ribosome-dependent Vibrio cholerae mRNAse HigB2 is regulated by a β-strand sliding mechanism. Nucleic Acids Res 45
23. Bakan A, Meireles LM, Bahar I (2011) *ProDy*: Protein Dynamics Inferred from Theory and Experiments. *Bioinformatics* 27, 1575–1577
24. Afif H, Allali N, Couturier M, Van Melderen L (2001) The ratio between CcdA and CcdB modulates the transcriptional repression of the ccd poison-antidote system. Mol Microbiol 41:73–82
25. Garcia-Pino A et al (2010) Allostery and Intrinsic Disorder Mediate Transcription Regulation by Conditional Cooperativity. Cell 142:101–111
26. Joung JK, Le LU, Hochschild A (1993) Synergistic activation of transcription by Escherichia coli cAMP receptor protein. *Proc. Natl. Acad. Sci. U. S. A.* 90, 3083–3087
27. Buchler NE, Gerland U, Hwa T (2003) On schemes of combinatorial transcription logic. *Proc. Natl. Acad. Sci. U. S. A.* 100, 5136–5141
28. Escalante-Chong R et al (2015) Galactose metabolic genes in yeast respond to a ratio of galactose and glucose. *Proceedings of the National Academy of Sciences* 112, 1636–1641
29. De Jonge N et al (2009) Rejuvenation of CcdB-Poisoned Gyrase by an Intrinsically Disordered Protein Domain. Mol Cell 35:154–163
30. Talavera A et al (2019) A dual role in regulation and toxicity for the disordered N-terminus of the toxin GraT. Nat Commun 10
31. Garcia-Pino A et al (2016) An intrinsically disordered entropic switch determines allostery in Phd–Doc regulation. Nat Chem Biol 12:490–496
32. Monti MC et al (2007) Interactions of Kid–Kis toxin–antitoxin complexes with the parD operator-promoter region of plasmid R1 are piloted by the Kis antitoxin and tuned by the stoichiometry of Kid–Kis oligomers. Nucleic Acids Res 35:1737–1749
33. Bøggild A et al (2012) The Crystal Structure of the Intact E. coli RelBE Toxin-Antitoxin Complex Provides the Structural Basis for Conditional Cooperativity. Structure 20:1641–1648
34. Winther KS, Gerdes K (2012) Regulation of Enteric vapBC Transcription: Induction by VapC Toxin Dimer-Breaking. Nucleic Acids Res 40:4347–4357
35. Jurėnas D, Van Melderen L, Garcia-Pino A (2019) Mechanism of regulation and neutralization of the AtaR–AtaT toxin–antitoxin system. Nat Chem Biol 15:285–294
36. Brown BL, Lord DM, Grigoriu S, Peti W, Page R (2013) The Escherichia coli Toxin MqsR Destabilizes the Transcriptional Repression Complex Formed between the Antitoxin MqsA and the mqsRA Operon Promoter. J Biol Chem 288:1286–1294

37. Pavelich IJ et al (2025) Antitoxin control of optimal transcriptional repression in the atypical HigB–HigA toxin–antitoxin system from *Proteus vulgaris*. Nucleic Acids Res 53
38. Zavrtanik U et al (2024) Leucine Motifs Stabilize Residual Helical Structure in Disordered Proteins. J Mol Biol 436:168444
39. Hadži S, Lah J (2022) The free energy folding penalty accompanying binding of intrinsically disordered α-helical motifs. Protein Sci 31
40. Teilum K, Olsen JG, Kragelund BB (2015) Globular and disordered—the non-identical twins in protein-protein interactions. Front Mol Biosci 2
41. Komives E, Sanchez-Rodriguez R, Taghavi H, Fuxreiter M (2024) Fuzzy protein-DNA interactions and beyond: A common theme in transcription? Curr Opin Struct Biol 89:102941
42. Sanborn AL et al (2021) Simple biochemical features underlie transcriptional activation domain diversity and dynamic, fuzzy binding to Mediator. *Elife* 10
43. Hadži S, Loris R, Lah J (2021) The sequence–ensemble relationship in fuzzy protein complexes. *Proceedings of the National Academy of Sciences* 118
44. Kussie PH et al (1996) Structure of the MDM2 Oncoprotein Bound to the p53 Tumor Suppressor Transactivation Domain. *Science (1979).* 274, 948–953
45. Chi S-W et al (2005) Structural Details on mdm2-p53 Interaction. J Biol Chem 280:38795–38802
46. De Guzman RN, Goto NK, Dyson HJ, Wright PE (2006) Structural Basis for Cooperative Transcription Factor Binding to the CBP Coactivator. J Mol Biol 355:1005–1013
47. Radhakrishnan I et al (1997) Solution Structure of the KIX Domain of CBP Bound to the Transactivation Domain of CREB: A Model for Activator:Coactivator Interactions. Cell 91:741–752
48. Tuttle AR, Trahan ND, Son MS (2021) Growth and Maintenance of *Escherichia coli* Laboratory Strains. Curr Protoc 1
49. Brzovic PS et al (2011) The Acidic Transcription Activator Gcn4 Binds the Mediator Subunit Gal11/Med15 Using a Simple Protein Interface Forming a Fuzzy Complex. Mol Cell 44:942–953
50. Thoden JB, Ryan LA, Reece RJ, Holden HM (2008) The Interaction between an Acidic Transcriptional Activator and Its Inhibitor. J Biol Chem 283:30266–30272
51. Kumar PR, Yu Y, Sternglanz R, Johnston SA & Joshua-Tor, L. NADP Regulates the Yeast *GAL* Induction System. *Science (*(1979)). 319, 1090–1092 (2008)). 319, 1090–1092 (2008)
52. Dosnon M et al (2015) Demonstration of a Folding after Binding Mechanism in the Recognition between the Measles Virus $N_{TAIL}$ and X Domains. ACS Chem Biol 10:795–802
53. Bignon C, Troilo F, Gianni S, Longhi S (2018) Modulation of Measles Virus NTAIL Interactions through Fuzziness and Sequence Features of Disordered Binding Sites. Biomolecules 9:8

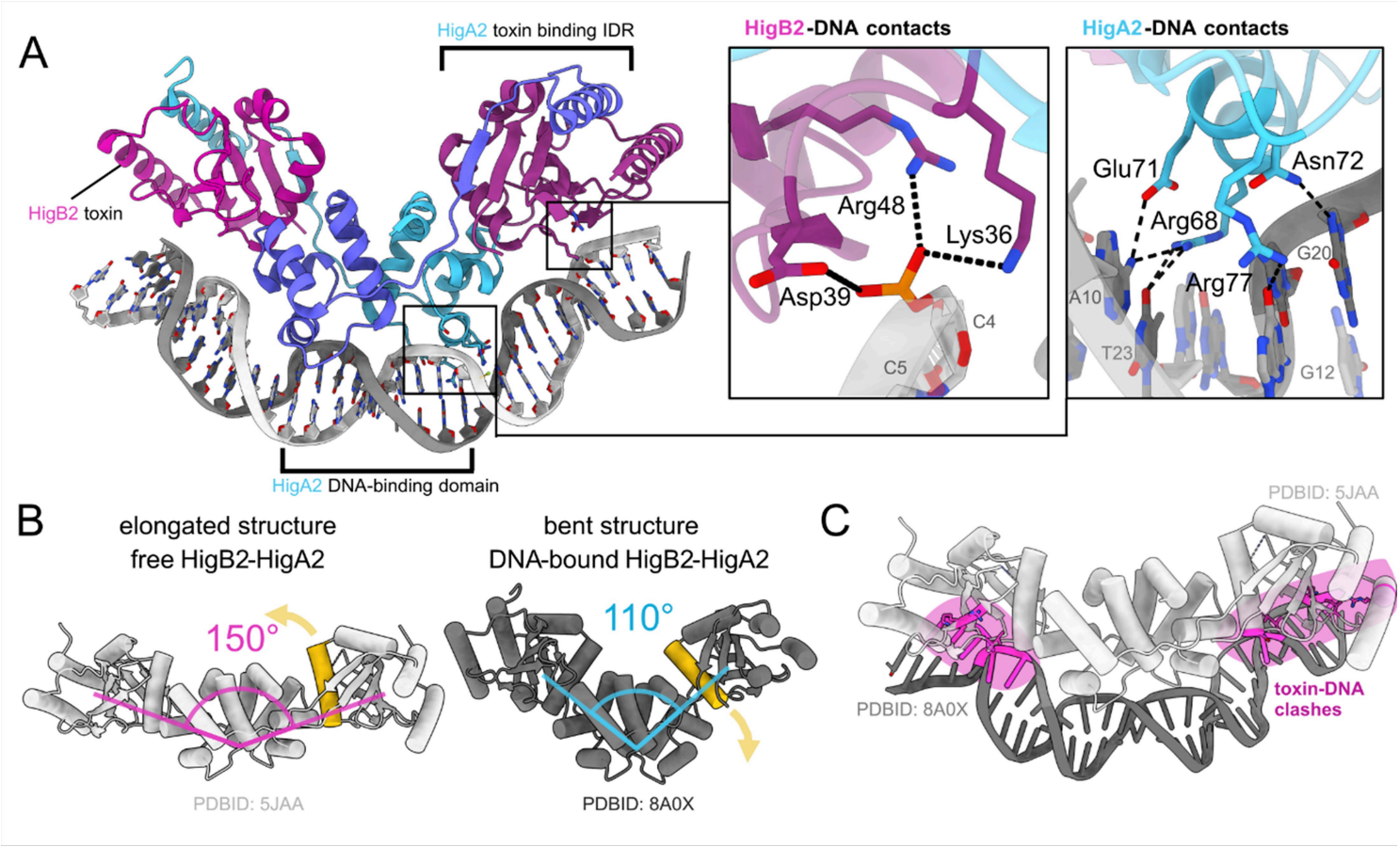
# Figures




## Figure 1

**HigB2 toxin acts as transcriptional de-repressor. A.** Schematic representation of the *wt higBA2* operon encoding HigB2 toxin (pink) and HigA2 antitoxin (blue). Closeup shows the single HigA2 binding site with two inverted repeats in bold, and a downstream toxin start codon (pink). **B.** Normalized fluorescence intensity ($FL/OD_{600}$) of batch experiments and **C.** single cell population distribution of cells expressing *mRFP1* under the $P_{higBA2}$ promoter (Ø, white) or with additional constitutively expressed toxin ($higB2_{Dloop}$, pink), antitoxin (*higA2*, blue) or both (*higB* higA2*, purple). Organization of the reporter system

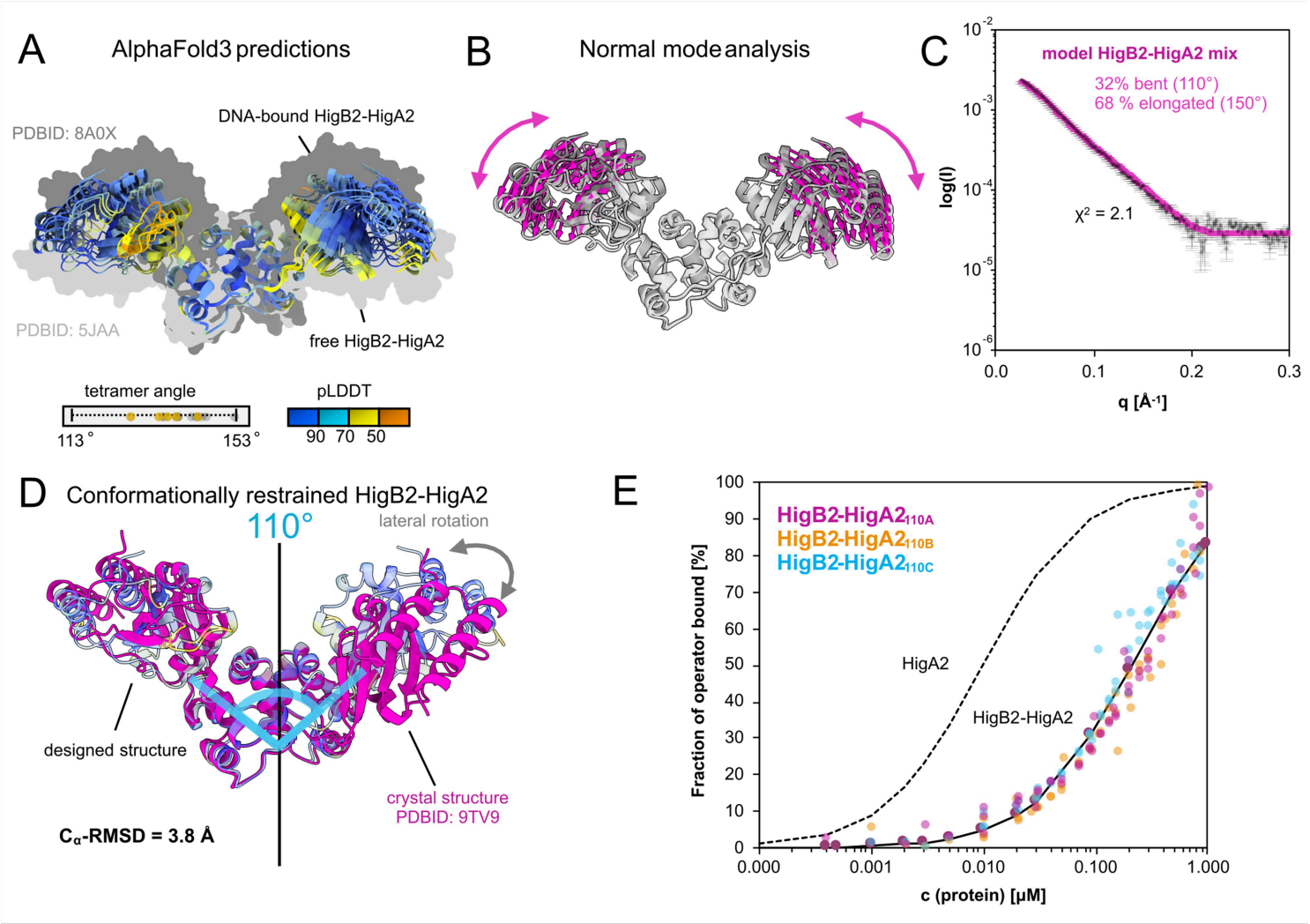
pSC1A3 for *in vivo* repression based on constitutive toxin and/or antitoxin expression is shown schematically above. Bars show the mean value from 6 ≤ n ≤ 15 independent experiments with errors corresponding to one s.d. **D.** Normalized fluorescence intensity for inducible *higB2* higA2* in the absence of inducer (uninduced, grey) in the presence of 30 μM IPTG with or without the addition of 100 μM L-arabinose (blue and pink, respectively). Black arrow denotes time of the addition of L-arabinose. Organization of the reporter system pRAT-sfGFP for *in vivo* repression based on inducible toxin and/or antitoxin expression is shown schematically above. **E.** EMSA for HigA2 antitoxin (blue) and HigB2-HigA2 complex (left, purple) binding to the operator fragment (Cy5-dsDNA45). Black arrows denote bands representing presumed DNA-protein complexes. **F.** Fluorescence anisotropy experiment for the HigA2 (blue) and HigB2-HigA2 (purple) binding to the operator fragment DNA45-Cy5. Fits of the binding isotherms are shown as black lines. Data shows a representative of 1 experiment with others shown in Supplementary Material (Figure S4).




## Figure 2

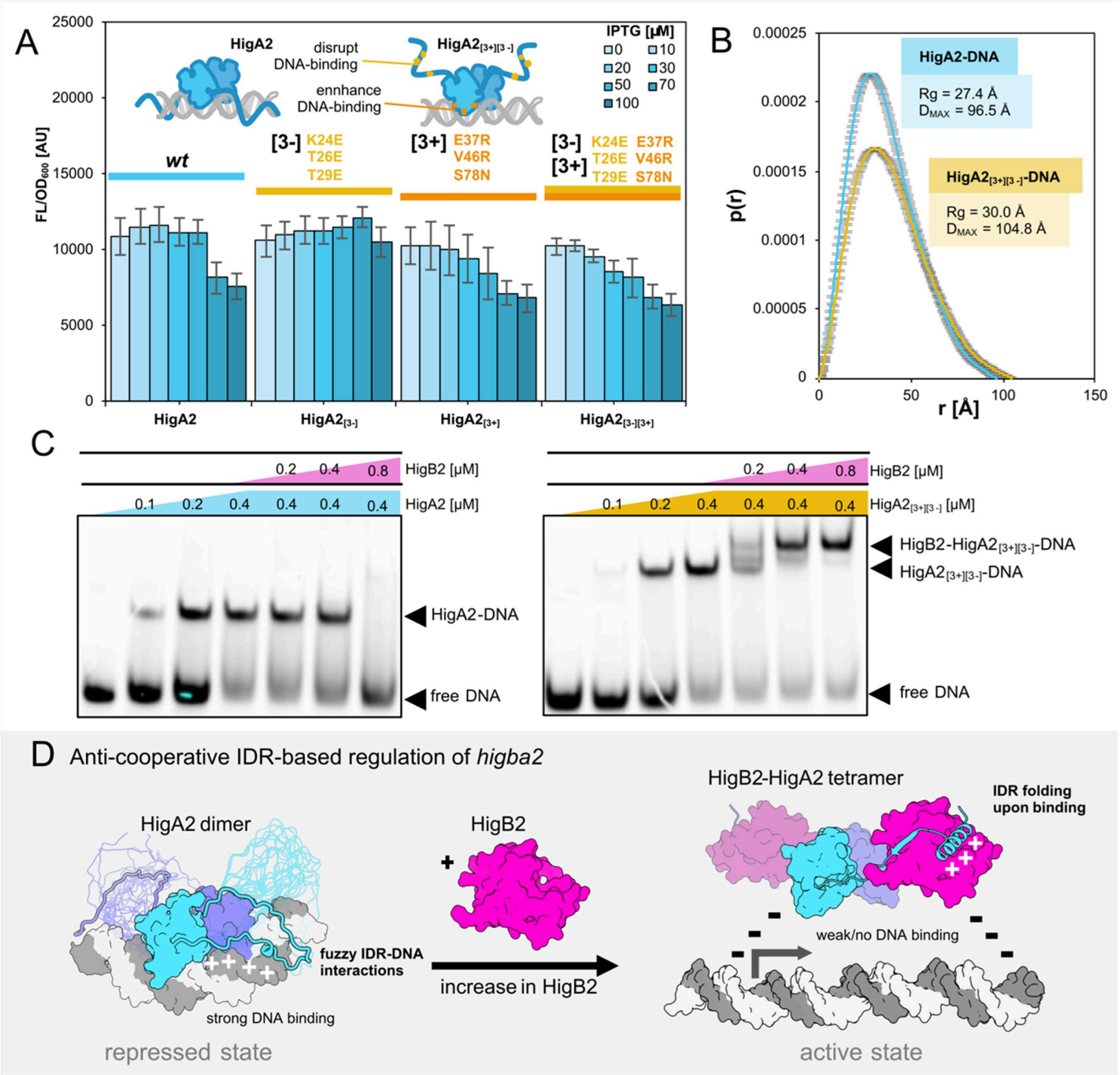
**Structure of the HigB2-HigA2-operator complex. A.** Crystal structure of the HigB2-HigA2 tetramer bound to the 31 base par long operator fragment (PDBID: 8A0X). Insets shows a closeup of toxin-DNA interactions (left) and antitoxin-DNA interactions (right). **B.**Comparison of the free HigB2-HigA2 tetramer (white, right, PDBID: 5JAA) and the DNA-bound (dark grey, left, PDBID: 8A0X) one. Change from the elongated (150°) into bend (110°) conformation consists of rigid body movement of HigB2 toxin helix 2 (shown in yellow) along the groove of the HigA2 antitoxin globular domain. **C.** The bending of the HigB2-

HigA2 tetramer is required to prevent steric clashes (pink) with the DNA molecule, as shown by the structural alignment of the elongated conformation (white, PDBID: 5JAA, aligned at α3 helix from the bend state).




## Figure 3

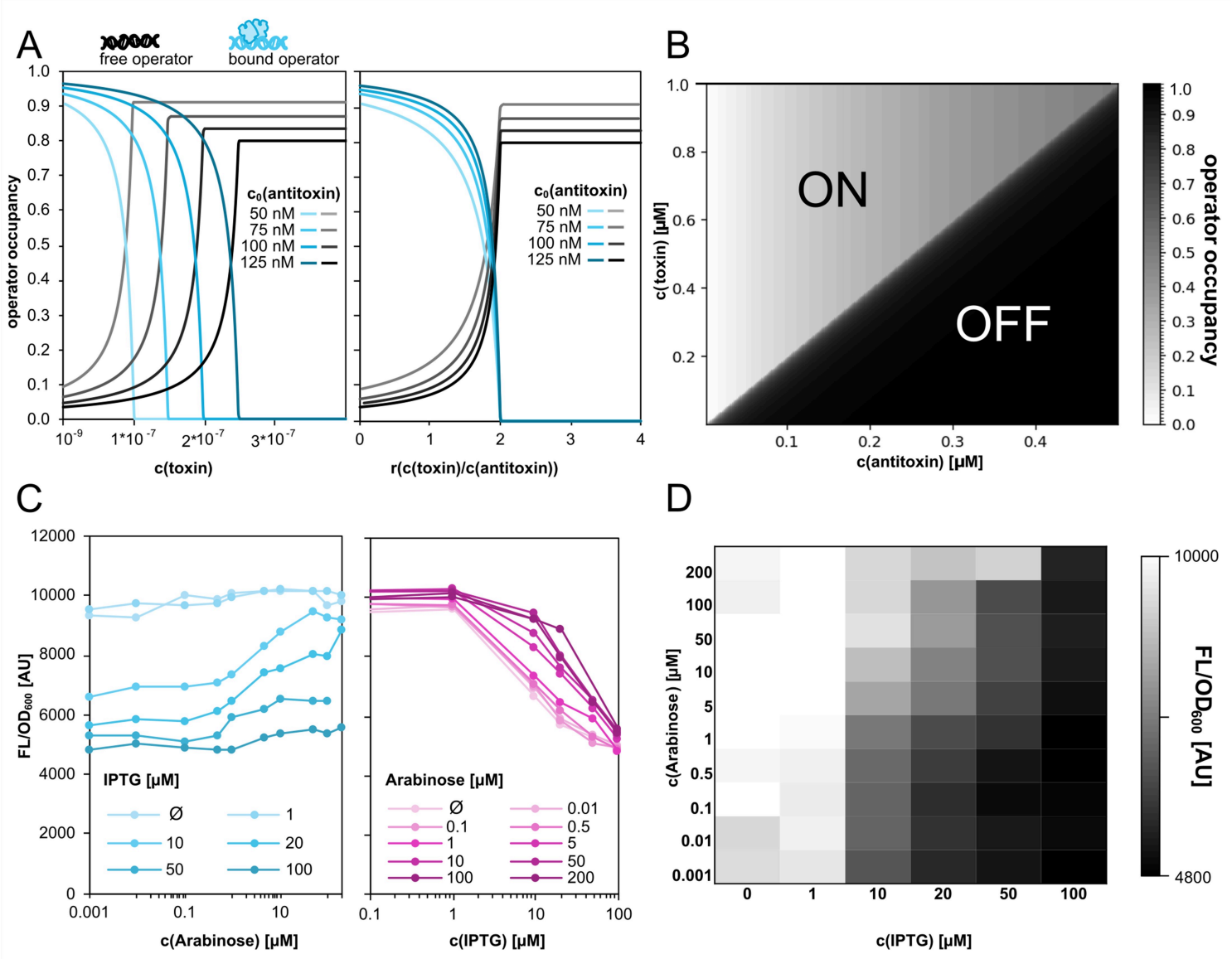
**HigB2-HigA2 conformational switch does not cause de-repression. A.** AlphaFold3 models of the HigB2-HigA2 tetramer (coloured by pLDDT score) compared to the conformation of free (white outline) and DNA-bound (grey outline) structure. Boxed plot shows the bending angle distribution of the five predicted models. **B.** Hinge-bending motion of HigB2-HigA2 tetramer corresponding to the largest normal mode revealed by the harmonic network analysis. **C.** SAXS data of HigB2-HigA2 tetramer (gray) and the corresponding OLIGOMER model fit (pink) for the mixture of elongated and bend confirmations. **D.** Comparison of the predicted (gray/blue) and experimental (pink, PDBID: 9TV9) structure of the HigB2-$HigA2_{110A}$ tetramer designed to adopt bent conformation, with the reported Cα atom RMSD for the left tetramer half. **E.** Fluorescence anisotropy experiment for the conformationally restrained tetramer variants binding to operator fragment DNA45-Cy5. For the reference the black line shows a fit of the 1:1 binding models of native HigA2 and HigB2-HigA2 from Figure 1.




## Figure 4

**Sequestering of HigA2 disordered domain by the HigB2 toxin mediates de-repression. A.** Repression of $P_{higBA2}$-*mRFP1* expression by HigA2 antitoxin variants designed to remove IDR-DNA fuzzy interactions ($HigA2_{[3-]}$ yellow), to enhance contacts between DNA-domain and operator ($HigA2_{[3+]}$ orange) or both ($HigA2_{[3+][3-]}$). Bars show normalized fluorescence ($FL/OD_{600}$) of cells expressing IPTG-inducible HigA2 and its variants in increasing concentrations of IPTG at 10 h post induction. **B.** Experimental distance distribution functions derived from the SAXS measurements of the HigA2-DNA (blue) and $HigA2_{[3+][3-]}$-

DNA (yellow) comperes, support less compact ensemble of the HigA2$_{[3+][3-]}$ variant. **C.** EMSA for binding of HigA2 (left, blue) and HigA2$_{[3+][3-]}$ (right, yellow) binding to DNA45-Cy5 with subsequent addition of toxin HigB2 (pink). Black arrows denote bands representing presumed DNA-protein complexes. **D.** Schematic representation of the anti-cooperative regulation mechanism of *higBA2* system based on IDR competition for binding to DNA operator or to HigB2 toxin. In the presence of HigB2 toxin, favourable IDR-DNA fuzzy interactions become substituted for IDR-toxin binding coupled with folding of IDR, leading to transcriptional de-repression.




## Figure 5

***higBA2* operon functions as a ratio-sensing autoregulatory circuit. A.** Equilibrium model of *higBA2* circuit parametrized with experimental affinities shows the release of the HigA2-bound operator (vertical axis) with the increasing concentration of HigB2 toxin (horizontal axis). The threshold HigB2 concertation required for switching depends on the initial amount of repressor HigA2 (left panel), which however occurs at the fixed HigB2/HigA2 molar ratio (right panel), independent of initial amount of

HigA2. **B.** Operator occupancy as a function of toxin and antitoxin concentration. Diagonal corresponds to the switching front at the constant 2:1 HigB2:HigA2 molar ratio **C.** Normalized fluorescence intensity of cells expressing sfGFP under $P_{higBA2}$ and different induction levels of HigA2 (using IPTG) and HigB2 (using arabinose) 20 hours post-induction. Toxin de-repression through arabinose induction at different levels of antitoxin expression is depicted in blue and the effect of antitoxin repression at different levels of toxin expression is depicted in pink. **D.** Ratio-dependent transcriptional regulation of the *higBA2* circuit. Heatmap shows the normalized fluorescence intensity at different levels of toxin and antitoxin expression, which agrees well with the results of quantitative model (panel B).

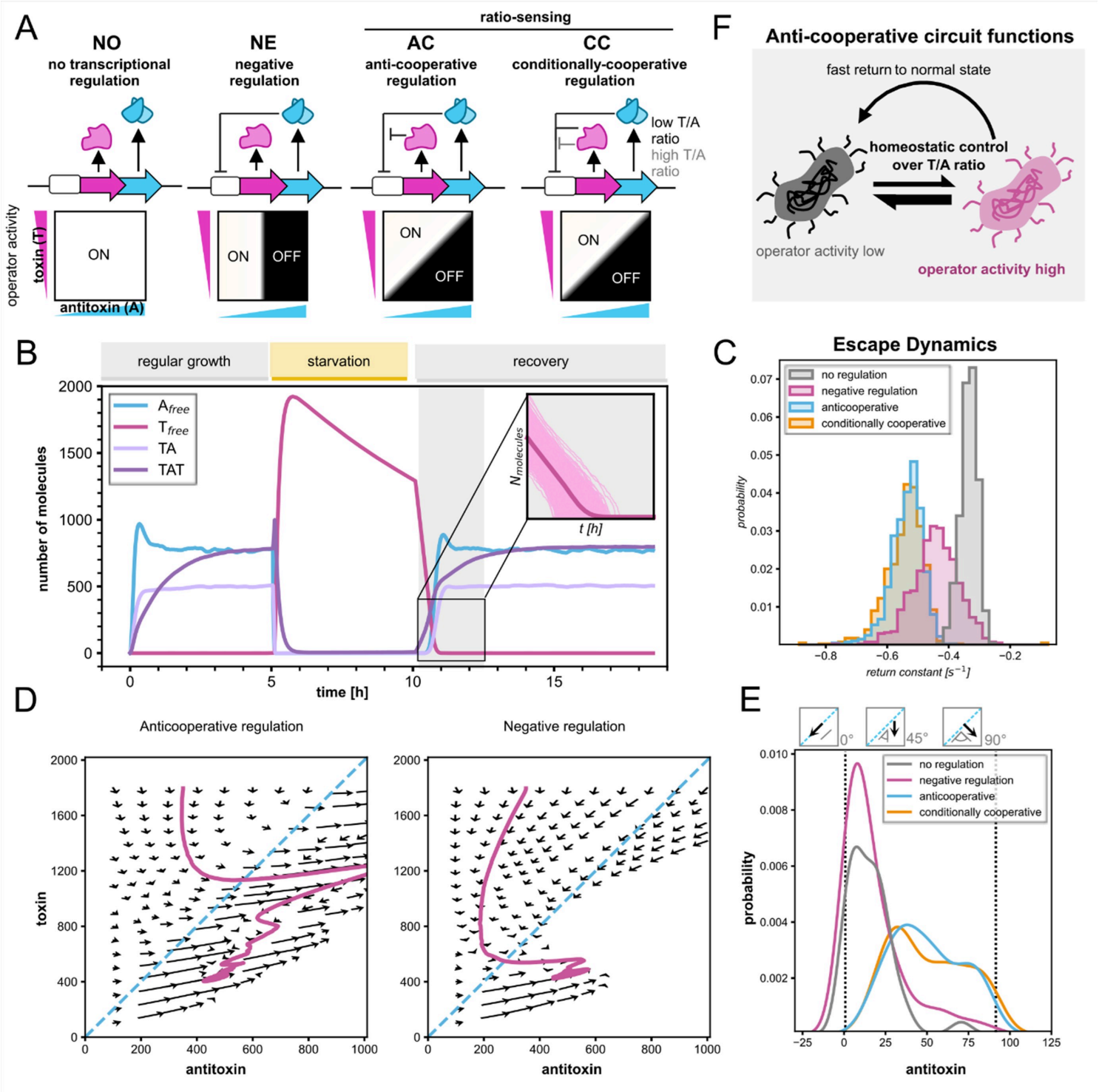


**Figure 6**

**Function of the anti-cooperative ratio-sensing circuit. A.** Schematic representation of four toxin-antitoxin autoregulation circuits (top) providing different two-dimensional outputs i.e. regulatory phenotypes (bottom). Ratio-dependent regulation is provided by anti-cooperative and conditional cooperativity provide. **B.** In stochastic kinetic simulations each system was let to evolve under normal growth regime, followed by a change in parameters (starvation regime between 5 to 10 hours), followed by a recovery. Traces show the time-dependence of the average number of proteins in cell for 1000 simulation runs for the AC circuit, as example. The inset shows a decrease in number of free toxin molecules during recovery for individual runs. **C.** Histograms compare the distributions of kinetic constants corresponding to toxin's decrease for different regulation mechanisms. **D.** Vector fields showing system's response upon perturbation of the steady-state concentrations of free toxin and antitoxin with pink line illustrating a selected trajectory. In case of the anti-cooperative regulation the response trajectories suggest initial decrease of the toxin:antitoxin ratio below 2:1 threshold, shown by blue dashed line. **E.** The distribution of vector angles for different regulation mechanisms. The 90 ° angles correspond to vectors pointing toward the 2:1 diagonal, corresponding to homeostatic control of the toxin:antitoxin ratio. **F.** Compared to simple negative feedback the functional advantage of ratio-dependent regulation mechanism entails homeostatic control over toxin/antitoxin levels and faster escape for the toxin-dominated. Functional performance of anti- and conditional cooperativity mechanisms is comparable.

## Supplementary Files

This is a list of supplementary files associated with this preprint. Click to download.

- SIzivc.pdf
- MovieS1.gif